Temperature Dependence of the Field-Effect Mobility of Sexithiophene. Determination of the Density of Traps

Gilles Horowitz, Riadh Hajlaoui, Philippe Delannoy

Classification
Physics Abstracts
72.20J — 72.80L — 73.60F

Temperature Dependence of the Field-Effect Mobility of Sexithiophene. Determination of the Density of Traps

Gilles Horowitz([1]), Riadh Hajlaoui([1]) and Philippe Delannoy([2])

([1]) Laboratoire des Matériaux Moléculaires, CNRS, 2 rue Henry-Dunant, 94320 Thiais, France
([2]) Groupe de Physique des Solides, Université Paris 7 - Denis Diderot, 75251 Paris Cedex 05, France

(Received 28 September 1994, accepted 3 January 1995)

Résumé. — La conductivité et la mobilité d'effet de champ du sexithiophène non substitué (6T) et du di-alkyl-sexithiophène substitué en bout de chaîne (DH6T) ont été mesurées en fonction de la température. Pour des températures supérieures à 150 K, on trouve une conductivité thermiquement activée, alors que la mobilité montre une énergie d'activation dépendante de la tension de grille. A forte tension de grille et à haute température, on observe une saturation de la mobilité d'effet de champ. Les données ont été analysées dans le cadre d'un modèle de piégeages et dépiégeages multiples. On a ainsi déterminé la distribution des niveaux localisés près de la bande de transport pour les deux produits. Cette distribution a été ajustée à une double exponentielle, par analogie avec celle du silicium amorphe hydrogéné (a-Si:H). Les pièges profonds dans 6T et DH6T sont associés aux joints de grain. La mobilité plus faible de 6T est attribuée à sa plus grande concentration de défauts. Pour les températures inférieures à 150 K, le transport par sauts thermiquement activés entre états localisés devient le mécanisme dominant. Cependant, le transport par piégeages et dépiégeages multiples peut de nouveau se manifester dans la couche d'accumulation d'un transistor à effet de champ fortement polarisé.

Abstract. — Conductivity and field-effect mobility measurements as a function of temperature have been carried out on unsubstituted sexithiophene (6T) and end-substituted dihexyl- sexithiophene (DH6T). At temperatures higher than 150 K, the conductivity is thermally activated, whereas the field-effect mobility presents a gate-bias dependent activation energy. Importantly, the field-effect mobility tends to saturate at both high gate voltages and high temperatures. The data were analyzed within the frame of a multiple thermal trapping and release model. The distribution of localized states near the transport level has been determined for both compounds, and was fitted to a double exponential distribution, which can be compared to that of hydrogenated amorphous silicon (a-Si:H). The localized trap states in 6T and DH6T originate from grain boundaries. The lower mobility of the unsubstituted compound can be attributed to the corresponding higher density of traps. At temperatures lower than 150 K, thermally activated hopping becomes the dominant transport mechanism, but multiple trapping can also be present in the accumulation layer of a field-effect transistor at high gate voltages.

1. Introduction

The use of organic materials as the active component in semiconductor devices has been studied for several decades. As organic semiconductors cannot be doped in both n- and p-type, the greatest part of the early works was devoted to Schottky (metal- semiconductor) diodes, most often in view of their use in photovoltaic devices [1,2]. Organic Schottky diodes have recently known a remarkable comeback when interest has focused on light-emitting diodes (LEDs) [3,4].

The history of organic field-effect transistors (OFETs) does not go back this far. Although a field-effect on polyacetylene (PA) thin film has been reported in 1983 [5], significant works on polymer field-effect transistors only emerged during the late eighties, when devices were made with the conjugated polymers PA [5,6], polythiophene (PT) [7,8] and poly(thienylene vinylene) (PTV) [9]. OFETs based on phthalocyanine compounds have also been reported [10]. It has been shown more recently that the performance of OFETs, and particularly their field-effect mobility μ_{FET}, can be significantly improved by replacing polymers by conjugated oligomers [11–13]. However, although values up to 3.0 $cm^2V^{-1}s^{-1}$ have been reported [13,14], the field-effect mobility of OFETs remains by far lower than that of conventional silicon FETs. This, of course, must be ascribed to the specific charge transport mechanism in organic materials. It is generally assumed that the charge carriers are not free to move in extended states, but are stored as polarons self-trapped into states localized in the forbidden band. Such localized states have been attested in conjugated oligomers [15,16] and polymers [17,18] by optical spectroscopy and electron spin resonance (ESR) measurements. The transport of polarons is dominated by hopping processes, and theories predict that their mobility should be strongly temperature dependent. A thermally activated mobility has indeed been reported in polythiophene [8] and sexithiophene OFETs [13]. We note however that, although the hopping distance R found in polythiophene compares well with the mean separation between dopant ions [8], its value in substituted oligothiophene is close to the distance between nearest-neighbor molecules [13], which is too small to be physically realistic.

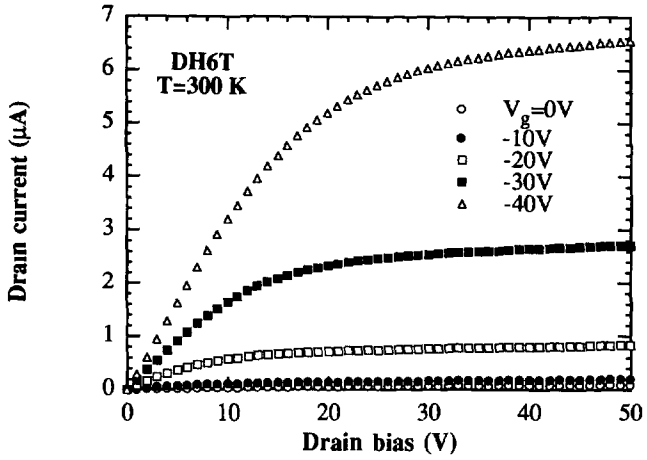

Fig. 1. — Drain-current vs. source-drain voltage curves for various gate biases measured on a dihexyl-sexithiophene (DH6T) organic field-effect transistor (OFET) at 300 K.

Figure 1 shows a set of drain current vs. drain bias ($I_d - V_d$) curves of a dihexyl-sexithiophene OFET recorded at 300 K for various gate voltages V_g. The device operates mainly in the enrichment mode, where carriers are injected in the semiconductor- insulator interface through the formation of an accumulation layer. The field-effect mobility can be estimated by the conventional equations of FETs, either from the saturation current $I_{d,sat}$, equation (1), or from the transconductance g_m at low drain current, equation (2) [19].

$$I_{d,sat} = \frac{W}{2L}\mu_{FET}C_i(V_g - V_0)^2, \tag{1}$$

$$g_m = \left(\frac{\partial I_d}{\partial V_g}\right)_{V_d \to 0} = \frac{W}{L}\mu_{FET}C_i V_d. \tag{2}$$

Here, W and L are the channel width and length, respectively; C_i is the insulator capacitance (per unit area) and V_0 the threshold voltage. The use of the transconductance, equation (2), presents the advantage of making the measurements at low drain biases, where the accumulation layer is almost uniform over the whole channel. The use of equation (1) on the set of characteristics in Figure 1 leads to a mobility of 3.8×10^{-2} $cm^2V^{-1}s^{-1}$ and a threshold voltage of 13.9 V. Such high values of V_0 are often encountered in OFETs. Equation (2) gives $\mu_{FET} = 2.3 \times 10^{-2}$ $cm^2V^{-1}s^{-1}$ for $V_d = -2$ V and $V_g \leq -25$ V.

Three years ago, we developed an analytical model for OFETs [20], based on an alternative charge transport model, the multiple trapping and release mechanism, which is generally invoked in the case of hydrogenated amorphous silicon (a-Si:H) [21]. In this model, most of the carriers injected in an organic semiconductor are trapped into states localized in the forbidden band. The conductivity σ is given by the concentration of free carriers n_f times a microscopic mobility μ_0, which is slowly varying with the temperature.

$$\sigma = n_f q\mu_0. \tag{3}$$

Here q is the absolute electron charge. Putting $\theta = n_f/n_{tot}$, where $n_{tot} = n_f + n_t$ is the total (free plus trapped) density of charges, we can write (3) as

$$\sigma = n_{tot} q\theta\mu_0. \tag{4}$$

Equation (4) shows that a thermally-activated conductivity can be interpreted, either by a thermally activated charge density $n_f = \theta n_{tot}$ and a constant mobility μ_0, or a thermally activated mobility $\mu = \theta\mu_0$ and a constant charge density n_{tot}. In reference [20], we assumed a trap distribution consisting of a shallow single level close to the main transport band (the conduction or valence band for classical n- and p-type semiconductors, respectively). In this case, the field-effect mobility at low-gate biases equals the effective mobility $\theta\mu_0$, and is hence thermally activated, whereas it approaches the slowly varying microscopic mobility μ_0 at high V_g. The predicted high gate voltage regime is similar to the trap-filled regime described by Lampert [22], where all traps are filled and any additional injected charge can move freely with the microscopic mobility. Our model was also able to explain the high threshold voltage often measured in OFETs, as noted above.

During the course of this work, Paloheimo and coworkers have reported the temperature dependent field-effect mobility of fullerene-based OFETs [23]. They found a thermally activated mobility at a fixed gate voltage, with an activation energy decreasing for increasing V_g. This strong gate voltage dependence was attributed to an exponential distribution of gap states, as is generally reported in a-Si:H. These results suggest that the determination of the trap density is a crucial step in OFETs' modelling.

In the present paper, we report on temperature dependent field-effect mobility measurements on OFETs made of unsubstituted and substituted sexithiophenes. A model is developed, which allows us to determine the localized trap distribution near the transport level.

2. Experimental

Figure 2 shows the molecular structure of sexithiophene (6T) and end-substituted dihexyl-sexithiophene (DH6T). The synthesis of these compounds has been extensively reported previously [24].

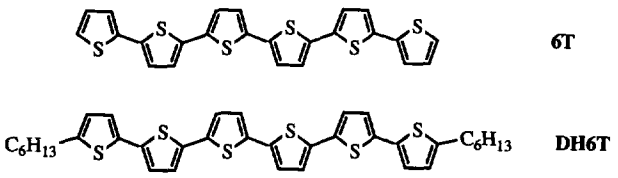

Fig. 2. — Extended molecular structure of sexithiophene (6T) and end-substituted dihexyl-sexithiophene (DH6T).

The field-effect transistors were fabricated according to a reversed architecture. First, the gate electrode (aluminum) is deposited on a glass substrate. The insulator consists of a 1 μm thick spin-coated poly(methylmetacrylate) (PMMA) layer. The organic semiconductor is vacuum-evaporated on top of the insulator, with a typical thickness of 100 nm. The evaporation was carried out at a rate of about 10 nm/s on substrates held at room temperature. Two gold stripes, 5 mm long and 100 μm wide, separated by 50 μm, form the source and drain electrodes. They are deposited either on top of the semiconducting layer, or between the insulator and the semiconductor, with equivalent results in both cases.

The current-voltage characteristics of the transistors were recorded with a Hewlett- Packard 4140B picoameter-dc voltage source. Low-temperature measurements were carried out under vacuum in a Displex (Air Product) closed-cycle cryostat. The transistor was placed on a home-made copper holder. The temperature was monitored with a APD-E digital temperature indicator-controller, equipped with a chromel-gold 0.07 atomic % iron thermocouple.

3. Method of Analysis

A method for determining the localized state distribution in a-Si:H has been previously developed by Spear and Le Comber [25]. The steps of the analysis are given hereafter. Although all the organic materials used here behave as p-type semiconductors, the equations will be more conveniently given for an n-type semiconductor. Their extension to p-type is straightforward. In most cases, this simply consists of changing the sign of the gate voltage V_g from positive for an n-type to negative in a p-type device. As we are dealing with wide band-gap semiconductors ($E_G \geq 2$ eV), minority carriers are neglected.

Figure 3 shows the energy scheme of the accumulation layer at the insulator-semiconductor interface with an applied source-gate bias V_g. The x-axis points perpendicular to the channel towards the bulk of the semiconductor, with its origin at the insulator-semiconductor interface. V_s is the value of the potential $V(x)$ at $x = 0$. The applied potential shifts the difference between

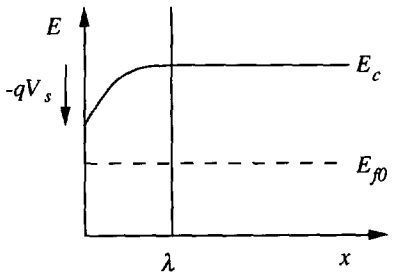

Fig. 3. — Energy scheme of the accumulation layer formed at the semiconductor surface in an OFET. The location of the Fermi level at the interface ($x = 0$) is $E_c - E_f = E_c - E_{f0} - qV_s$. λ corresponds to the thickness of the accumulation layer. The scheme is drawn for an n-type semiconductor.

the transport band edge and the Fermi level at $x = 0$ from $E_c - E_{f0}$ to $E_c - E_f = E_c - E_{f0} - qV_s$. As the potential drop in the semiconductor accumulation layer cannot exceed $E_c - E_{f0}$, V_s is generally much lower than $V_g - V_{fb}$, where V_{fb} is the flat-band potential, and the total surface charge Q_{tot} induced by the gate bias is very close to

$$Q_{tot} = -C_i(V_g - V_{fb}), \tag{5}$$

where C_i is the capacitance, per unit area, of the insulating layer. This total charge will split in two parts, a trapped charge Q_t and a free charge Q_f. The field-effect mobility given by equation (2) corresponds to the free surface charge:

$$\mu_{FET} = \mu_0 \frac{|Q_t|}{|Q_{tot}|}. \tag{6}$$

In order to calculate the free surface charge Q_f, we have to know the spatial charge distribution in the accumulation layer. In the original paper by Spear and Le Comber [25], it was assumed that, as most of the charge is trapped in localized states, the space charge of free carriers can be neglected, and the charge in the accumulation layer can be taken as constant up to a distance λ from the semiconductor surface, and zero beyond λ (abrupt approximation). The potential $V(x)$ is then in the form of a parabolic Schottky barrier:

$$V(x) = V_s \left(1 - \frac{x}{\lambda}\right)^2, \tag{7}$$

with

$$V_s = \lambda \frac{|Q_t|}{2\varepsilon_s} \approx \lambda \frac{C_i(V_g - V_{fb})}{2\varepsilon_s}. \tag{8}$$

Here ε_s is the dielectric constant of the semiconductor. We note that the assumption of a constant trapped carrier density is contradictory with a bias dependent distribution of localized states $N_t(E)$. The method by Spear and Le Comber has been more recently analyzed by Powell [26], who concluded that, "Only the broad feature of the density of states can be determined from field-effect conductance measurements". He also showed that the net effect of the abrupt approximation is an underestimation of the trap density by a factor of 4 at most. In the Appendix, we calculate the exact spatial distribution of trapped charges for the case of an exponential distribution of traps.

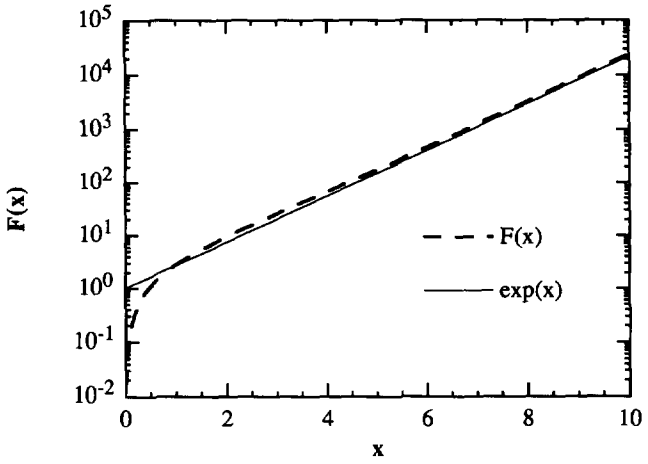

Fig. 4. — Numerical computation of the function $F(x) = \sqrt{x}\int_0^x \frac{e^x}{\sqrt{u}}\,du$. The function e^x, which is the limit of $F(x)$ at high x's is shown for comparison.

The free surface charge is now obtained by integrating the free carrier concentration n_f over the accumulation layer

$$|Q_f| = q\int_0^\lambda n_f(x)dx = qn_b\int_0^\lambda \exp\frac{qV(x)}{kT}dx. \tag{9}$$

Here, $n_b = N_c \exp[-(E_c - E_{f0})/kT]$ is the concentration of free carriers in the bulk of the semiconductor. N_c is the effective density of state in the conduction level, k the Boltzman constant and T the absolute temperature. Introducing the dimensionless variable $u = qV/kT$, equation (9) can be written as:

$$|Q_f| = qn_b\int_0^\lambda \exp\ u(x)dx. \tag{10}$$

which can be integrated as:

$$\frac{|Q_f|\,C_i(V_g - V_{fb})}{kT\varepsilon_s n_b} = \sqrt{u_s}\int_0^{u_s}\frac{e^u}{\sqrt{u}}du = F(u_s) \tag{11}$$

A numerical computation of the function $F(x)$ is given in Figure 4. By replacing the exponential by its Taylor's series, it can be easily shown that for $x > 1$, $F(x) \approx \exp(x)$. Making use of equations (5) and (6), equation (11) simplifies to

$$qV_s \approx E_c - E_{f0} - kT\ln\left[\frac{\mu_0 N_c kT\varepsilon_s}{\mu_{FET}C_i^2(V_g - V_{fb})^2}\right]. \tag{12}$$

Equation (12) allows us to estimate V_s as a function of the gate voltage, from which the difference between the Fermi level and the conduction band edge at the semiconductor surface can be computed. We can also calculate the density of trapped carriers n_t as a function of V_g:

$$qn_t = \frac{|Q_t|}{\lambda} \approx \frac{C_i^2(V_g - V_{fb})^2}{2\varepsilon_s V_s}. \tag{13}$$

We have assumed here that $Q_t \approx Q_{tot}$. The thickness of the accumulation layer λ was obtained from equation (8) and n_t is related to the density of localized states N_t through:

$$n_t(E_f) = \int_{-\infty}^{\infty} \frac{N_t(E)dE}{1 + \exp\dfrac{E - E_f}{kT}}. \tag{14}$$

In the case of a slowly varying trap distribution, the Fermi distribution can be approximated to a step function and equation (14) reduces to

$$n_t(E_f) \approx \int_{-\infty}^{E_f} N_t(E)dE, \tag{15}$$

which can be derived to

$$N_t(E) = \frac{dn_t}{dE}. \tag{16}$$

The steps of the analysis can be summarized as follows.

a) Determine the field-effect mobility from the gate-voltage dependent drain current at low source-drain bias through equation (2). We stress that the use of equation (2) in place of equation (1) leads to a gate voltage dependent mobility. Moreover, equation (2) allowed us to calculate μ_{FET} even when equation (1) is not followed, e.g., at low temperature (see below).

b) Calculate V_s using equation (12). The product $\mu_0 N_c$ appears as an adjustable parameter, the determination of which will be discussed further. Then calculate $E_c - E_{f0}$. As will be shown later on, the Fermi level at equilibrium is deduced from the temperature-dependent conductivity.

c) Calculate the concentration of trap carriers n_t using equation (13). The density of localized states N_t is then obtained through a numerical derivation of n_t as a function of $E_c - E_f$.

4. Results

The $I_d - V_d$ characteristics at 100 K of the same OFET as in Figure 1 are shown in Figure 5. At this temperature, we still observe clear linear and saturation regimes, but we note that the gate bias dependence of the drain current is much steeper than at room temperature. Particularly, the square-root dependence of the saturation current as a function of V_g predicted by equation (1) is no longer observed, which prevents the determining of a threshold voltage. Figure 6 shows the variation of the field-effect mobility of DH6T as a function of the gate voltage (6a) and temperature (6b). We have drawn the temperature dependence in an Arrhenius plot. We note that the curves are not really good straight lines. Classical hopping models lead to a linear variation of $\log\mu$ as a function of $T^{-\alpha}$. A value of α close to 1/4 is attributed to variable range hopping, and a value close to 1/2 to Coulomb interactions [27]. Attempts made to plot $\log\mu_{FET}$ against $T^{-0.5}$ and $T^{-0.25}$, did not lead to a clear improvement of the linearity. Importantly, the field-effect mobility is strongly gate bias dependent at low temperatures, whereas μ_{FET} approaches a constant value of about 0.04 $cm^2V^{-1}s^{-1}$ at both high temperatures and high gate voltages.

The analysis developed in the previous section was used to determine the localized state distribution $N_t(E)$. Calculations were made for gate biases higher than 10 V, so that we could

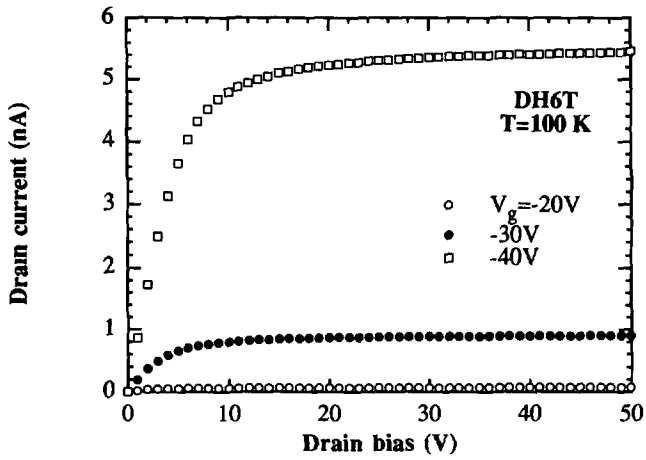

Fig. 5. — Same as Figure 1 measured at 100 K. Note the different current scale.

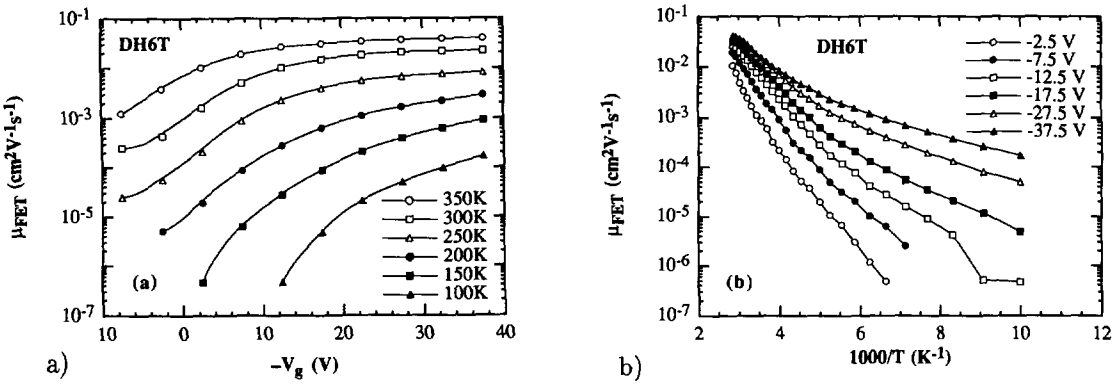

Fig. 6. — Gate bias and temperature dependence of the field-effect mobility in a dihexyl-sexithiophene OFET. Curves are plotted as a function of the gate bias for various temperatures (a), and as the function of the reversed temperature for various gate biases (b).

neglect the flat-band potential correction. The position of the Fermi level at equilibrium was deduced from the temperature dependent conductivity, Figure 7. We have already reported on the strong anisotropy of the conductivity of DH6T thin films [24]. As field-effect mobility measurements deal with the parallel component of the charge transport, we present here results for the parallel conductivity. The Arrhenius plot shows a constant activation energy $\Delta E = 0.22$ eV in the medium range (145 K< T < 230 K), whereas the variation tends to slow down at both higher and lower temperatures. We note again that attempts to improve the linearity by plotting logσ against $T^{-0.5}$ or $T^{-0.25}$ did not clearly succeed.

Several routes can be followed for estimating the $\mu_0 N_c$ product. We note that, owing to its logarithmic dependence in equation (12), a variation of $\mu_0 N_c$ by one order of magnitude will only induce a shift in V_s by $2.3 \times kT/q$ (i.e., 59 mV at room temperature, and even less at lower temperatures). The effective density of states N_c can be taken as the total density of molecules, as is usually done in narrow band materials. From X-ray diffraction

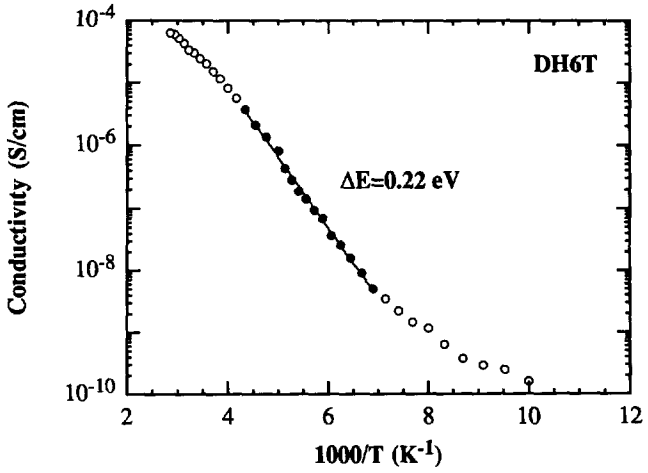

Fig. 7. — Arrhenius plot of the parallel conductivity of a vacuum evaporated DH6T thin solid film.

measurements reported in references [24] and [28], the crystal density of DH6T (molecular weight: 664) and 6T (molecular weight: 494) have been determined as 1.44 and 1.50 g/cm^3 in polycrystalline films, corresponding to a molecular density of 1.3×10^{21} and 1.8×10^{21} cm^{-3}, respectively. The actual density of an evaporated film of 6T does not differ by more than 10% from its crytallographic density [29]. In the case of DH6T, the microscopic mobility can be taken as the limit of μ_{FET} at high temperatures and gate biases. An alternative route for determining $\mu_0 N_c$ consists of minimizing the scattering of the trap distributions calculated at various temperatures. Although this leads to somewhat cumbersome computations, we finally chose this last solution, owing to that a high temperature limit of the mobility could not be obtained in the case of unsubstituted 6T.

The calculated density of localized states in DH6T is given in Figure 8. Data at 40 and 100 K extend more towards the transport level, owing to the fact that measurements at these temperatures were made at higher gate voltages. The best matching of the distributions obtained at various temperatures was obtained with $\mu_0 N_c = 2.5 \times 10^{19}$ (cmVs)$^{-1}$, a value twice lower than that given by multiplying the molecular concentration by the high gate voltage limit of μ_{FET}. As the microscopic mobility cannot be less than the field-effect mobility, we conclude that the effective density of state is half the molecular density. We note a strong deviation from the general trend of the data at 40 K, and a weaker one at 100 K, the deviation being more pronounced as the distance from the transport band edge increases. The strongest discrepancy corresponds to measurements carried out at lower gate voltages. The higher the gate bias is, the closer the data to the band edge and the smaller the temperature deviation.

A similar analysis was made for the unsubstituted oligomer 6T. Again, the position of the Fermi level at equilibrium, $E_c - E_{f0} = 0.26$ eV, was deduced from the temperature dependent conductivity, Figure 9. The results of the analysis are shown in Figure 10. The optimum agreement of the data at various temperatures was obtained with a $\mu_0 N_c$ product of 3×10^{19} (cmVs)$^{-1}$ If we assume, like in the case of DH6T, that the effective density of state equals half the molecular density, this gives us a microscopic mobility of 0.03 cm^{2}V^{-1}s^{-1}, almost identical to that of DH6T. We again note a small departure of the data at 70 K from the general trend.

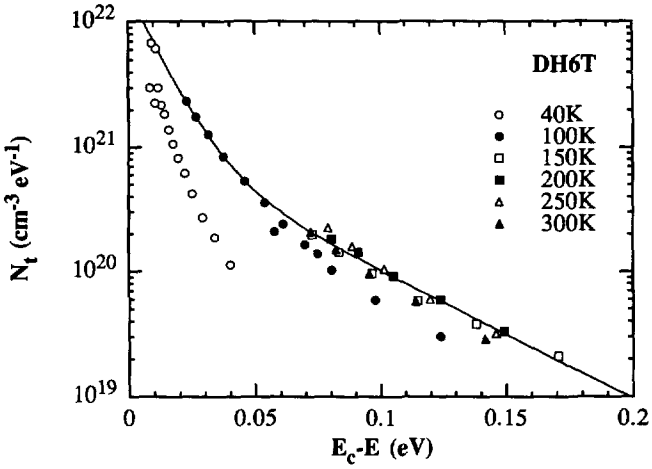

Fig. 8. — Localized state distribution of DH6T as deduced from field-effect measurements at various temperatures.

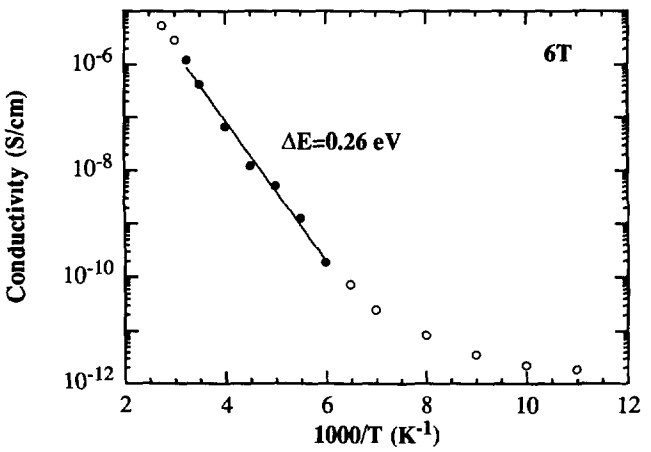

Fig. 9. — Temperature dependence of the parallel conductivity of unsusbstituted 6T.

5. Discussion

We consider an exponential distribution of localized states:

$$N_t(E) = \frac{N_{t0}}{kT_c} \exp\left(-\frac{E_c - E}{kT_c}\right). \tag{17}$$

Here, N_{t0} is the total density of traps and T_c the characteristic temperature of the distribution. In a-Si:H, the actual localized state distribution may be divided into deep states and tail states, each of which can be approximated to an exponential distribution [30]. Figure 8 shows clearly that the trap distribution in DH6T can be fitted also to a double exponential. Values of the parameters are gathered in Table I. Those of a-Si:H are given for comparison. In the case of 6T, the data were fitted to a single exponential, corresponding to the deep-state

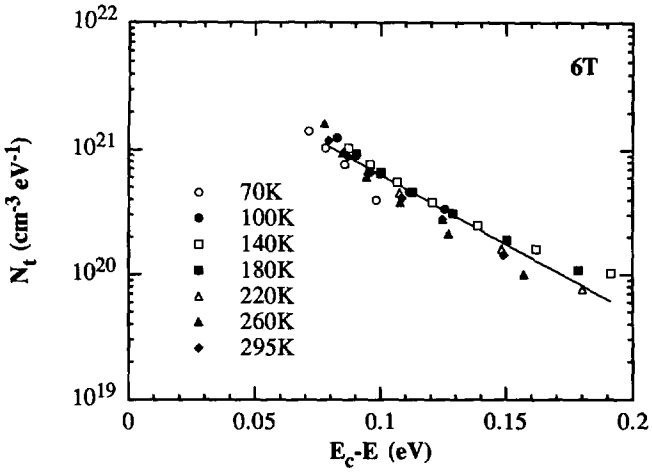

Fig. 10. — Same as Figure 8 for unsubstituted sexithiophene (6T).

Table I. — *Parameters of the trap distribution of sexithiophene (6T), dihexyl-sexithiophene (DH6T), and hydrogenated amorphous silicon (a-Si:H). T_c: characteristic temperature of the distribution; N_{t0}. density of states of the distribution. Data for a-Si:H taken from reference [30].*

			6T	DH6T	a-Si:H
Molecular density		(cm^{-3})	1.8×10^{21}	1.3×10^{21}	5.0×10^{22}
Effective density of states		(cm^{-3})	9×10^{20}	6.5×10^{20}	7×10^{19}
Microscopic mobility		(cm^{2}V^{-1}s^{-1})	0.03	0.04	17
Deep states	T_c	(K)	455	495	1000
	N_{t0}	(cm^{-3})	3×10^{20}	4.5×10^{19}	4×10^{17}
Tail states	T_c	(K)	120		260
	N_{t0}	(cm^{-3})	2×10^{20}		1×10^{20}
Dopant concentration		(cm^{-3})	4×10^{17}	3×10^{17}	—

distribution. We note that both the deep and tail states have a narrower distribution in the case of sexithiophenes than in a-Si:H. Deep states in a-Si:H originate from dangling bonds. In sexithiophenes, they most probably come from grain-boundaries, as X-ray measurements and electron microscope observation show that thin solid films of these materials are polycrystallines. Moreover, scanning electron micrography (SEM) reveals that the grain size is higher in DH6T than in 6T [31], which is consistent with the higher density of deep states in the unsubstituted compound. However, as SEM observation only gives a two-dimensional view of the grains, a quantitative correlation between grain size and trap density would be speculative.

Although the tail-state distribution could not be accessed in 6T, we can reasonably assume

that it is identical in both compounds. One of the most interesting feature in Table I is that 6T and DH6T have almost identical microscopic mobilities, which means that the lower field-effect mobility of the unsubstituted compound at room temperature is fully ascribed to its higher density of deep states. μ_{FET} is expected to approach the microscopic mobility when T approaches T_c. The reaching of the microscopic mobility with 6T would require measurements at temperatures closer to T_c, which is prevented by degradations of the organic material at $T > 350$ K.

Assuming the Fermi level at equilibrium E_{f0} to be located within the deep-state distribution, we can estimate E_{f0} by writing the electrical neutrality of the semiconductor. As the actual conductivity of sexithiophene films is much greater than their intinsic conductivity, we assume that thermal carriers are brought by a single shallow donor level of density N_d located at an energy E_d close to the transport level. Assuming again that the density of trapped carriers is much higher than that of the free carriers, the electrical neutrality writes

$$N_d^+ = n_t$$

or

$$N_d \left[1 - \left(1 + \exp \frac{E_d - E_{f0}}{kT}\right)^{-1}\right] = N_{t0} \exp\left(-\frac{E_c - E_{f0}}{kT_c}\right). \tag{18}$$

Putting $X = \exp[(E_c - E_{f0})/kT_c]$ and $l = T_c/T$, equation (18) reduces to

$$X^{l+1} - \frac{N_{t0}}{N_d}\left[X^l + \exp\left(\frac{E_c - E_d}{kT}\right)\right] = 0. \tag{19}$$

For a shallow donor level, $E_c - E_d < E_c - E_{f0}$ and equation (19) simplifies to

$$X = \frac{N_{t0}}{N_d}.$$

The position of the Fermi level at equilibrium is given by

$$E_c - E_{f0} = kT_c \ln \frac{N_{t0}}{N_d}, \tag{20}$$

which is independent of the temperature, and the conductivity by

$$\sigma = qn_f\mu_0 = qN_c\mu_0 \exp\left(-\frac{E_c - E_{f0}}{kT}\right) \tag{21}$$

From equation (20) a dopant concentration $N_d = 4 \times 10^{17}$ cm^{-3} is obtained for 6T, and 3×10^{17} cm^{-3} for DH6T, in good agreement with the value deduced from capacitance-voltage measurements on Schottky diodes. A value of about 10^{18} cm^{-3} has also been recently deduced from ESR measurements on 6T and DH6T solid films [32]. We stress that, within the multiple trapping and release model, this density corresponds to the total (free and trapped) density of charge carriers.

On the high temperature (left hand) side of Figure 7, the slight deviation from the Arrhenius plot of $\sigma(T)$ can be ascribed to that, as T approaches T_c, the trap distribution width approaches that of the Fermi distribution. Accordingly, the density of free carriers approaches that of the trapped carriers, and the conductivity saturates to a constant value $\sigma_\infty = N_d q\mu_0 \approx 0.002$ S/cm, a value that would be reached at $T_\infty = 550$ K.

When temperature decreases, the probability of thermal release from the localized traps decreases, and thermally activated hopping between trap sites will eventually become the dominant transport mechanism [21]. This can account for the change of the slope in Figures 7 and 9 at low temperatures. A transition from trapping to thermally activated hopping at about 150 K can also account for the deviation of the density of traps deduced from the field-effect measurements at temperatures lower than 150 K. Importantly, a backward transition from hopping to trapping can also be induced in the accumulation layer by increasing the gate voltage. As V_g increases, more trap levels are filled with injected charges. Eventually, all the deep traps will be filled, and the dominant transport mechanism will be switched back to multiple trapping. Evidence for such a transition is the very fast increase of the saturation current with the gate voltage at low temperature, and also that at high gate voltages (i.e., at energies close to the transport band edge), the trap density measured at low temperature tends to merge with that obtained at high temperatures.

In all our analysis, we have assumed that the microscopic mobility μ_0 was independent of the temperature. It is known, from time of flight (TOF) measurements on single crystalline organic semiconductor that the temperature dependence of the microscopic mobility has the general form

$$\mu_0 = \mu_{00} T^{-n}, \tag{22}$$

where n ranges between 1.5 and 2 [33]. For measurements between 100 and 300 K, such a dependence induces a change of μ_0 by a factor of less than 10, which is far smaller than the actual variations of μ_{FET} reported here, Figure 6. Any slow variation of the microscopic mobility is hence hidden by the much faster variation of the density of free carriers.

We note however that the microscopic mobility of sexithiophenes is small, and the corresponding mean free paths not longer than a lattice constant [13], which is not consistent with a transport in delocalized states. Low mobilities are generally interpreted within the frame of the thermally activated hopping transport, where the mobility is expressed as $\mu = \mu_0 \exp(-T_0/T)^n$, with $n = 1$, 0.5 or 0.25, depending on the hopping mechanism. Such a hopping mechanism is likely in sexithiophene at low temperatures, but can be excluded at higher temperatures, where the activation energy of the mobility is lower than that of the conductivity, and is strongly gate bias dependent. These two features have been successfully rationalized here by a multiple trapping and release mechanism. We note that theories based on a molecular polaron concept, recently developed by Silinsh and coworkers [34], could account for the charge transport in molecular crystals, where non thermally activated mobilities are associated with mean free paths not longer than the intermolecular distance.

6. Conclusion

We have used a multiple trapping and release model to analyze the temperature dependence of the conductivity and field-effect mobility of the unsubstituted and an end-substituted sexithiophenes. We found in both cases that the data lead to a distribution of localized states that can be fitted to a double exponential distribution. The model is able to account for both the thermally activated conductivity, down to about 150 K, and the gate bias dependent activation energy of the field-effect mobility. Both the unsubstituted and the end-substituted compounds are found to have almost similar microscopic mobilities. The ten-times lower field-effect mobility of 6T at room temperature can be entirely ascribed to its higher density of deep traps. At temperatures lower than 150 K, a thermally-activated hopping mechanism could be invoked to account for the change in the temperature dependence of the conductivity. The rather low microscopic mobility could be accounted for by a model recently developed by Silinsh

and coworkers, in which the molecular polaron "may be regarded as a slightly delocalized ionic state which moves by hopping via tunneling from one site to another" [34], a mechanism which, unlike thermally-activated hopping, is temperature-independent.

Appendix A

We calculate here the spatial distribution of trapped charges for the exponential distribution of traps given by equation (17). Again, the calculations are given for an n- type semiconductor, and minority carriers are neglected. By making use of equation (A.1)

$$F = -\frac{\mathrm{d}V}{\mathrm{d}x} \tag{A.1}$$

Poisson's equation

$$\frac{\mathrm{d}F}{\mathrm{d}x} = \frac{\rho_{\mathrm{tot}}}{\varepsilon_{\mathrm{s}}} \tag{A.2}$$

where F is the electric field along the x direction, can be integrated to

$$F^2 = -\frac{2}{\varepsilon_{\mathrm{s}}} \int_0^V \rho_{\mathrm{tot}} \mathrm{d}V' \tag{A.3}$$

We now assume that practically all charges are trapped, so that

$$\rho_{\mathrm{tot}} \approx -q n_{\mathrm{tb}} \exp \frac{qV}{kT_{\mathrm{c}}} \tag{A.4}$$

where $n_{\mathrm{tb}} = N_{\mathrm{t}} \exp[-(E_{\mathrm{c}} - E_{\mathrm{f0}})/kT_{\mathrm{c}}]$. Equation (A.3) now writes

$$F^2 = \frac{2kT_{\mathrm{c}} n_{\mathrm{tb}}}{\varepsilon_{\mathrm{s}}} \left(\mathrm{e}^{\frac{u}{l}} - \frac{u}{l} - 1 \right) \tag{A.5}$$

where $u = qV/kT$ and $l = T_{\mathrm{c}}/T$. In the accumulation regime, the exponential term dominates and one has

$$F \approx \sqrt{\frac{2kT_{\mathrm{c}} n_{\mathrm{tb}}}{\varepsilon_{\mathrm{s}}}} \exp \frac{qV}{2kT_{\mathrm{c}}} \tag{A.6}$$

The spatial distribution of free carriers can now be derived by writing (A.1) as

$$\mathrm{d}x = -\frac{\mathrm{d}V}{F}$$

and integrating from the surface ($x = 0$ and $V = V_{\mathrm{s}}$):

$$x = \int_0^x \mathrm{d}x' = -\int_{V_{\mathrm{s}}}^V \frac{\mathrm{d}V'}{F} \tag{A.7}$$

From (A.6) and (A.7) we get

$$x = \sqrt{\frac{2kT\varepsilon_{\mathrm{s}}}{q^2 n_{\mathrm{tb}}}} \left[\exp\left(-\frac{qV}{kT_{\mathrm{c}}} \right) - \exp\left(-\frac{qV_{\mathrm{s}}}{kT_{\mathrm{c}}} \right) \right] \tag{A.8}$$

The term $\exp(-qV_s/kT_c)$ is related to the total induced charge $Q_{tot} = -C_i(V_g - V_{fb})$ through equation (A.6) and Gauss's law

$$\varepsilon_s F_s = -Q_{tot} = C_i(V_g - V_{fb}) \tag{A.9}$$

where F_s is the value of F at the semiconductor surface. The spatial distribution of trapped charges can now be derived from (A.4) and (A.8)

$$n_t(x) = \frac{2kT_c\varepsilon_s}{q^2(x + x_{0t})^2} \tag{A.10}$$

where

$$x_{0t} = \frac{2kT_c\varepsilon_s}{qC_i(V_g - V_{fb})} \tag{A.11}$$

This carrier density profile has the same analytical expression as that derived from the well-known Mott-Gurney potential [35]. Obviously, it strongly differs from the constant distribution that we used in the text. We can however show that both distributions correspond to practically identical surface potentials V_s.

In order to calculate V_s, we first derivate a general expression for the free surface charge Q_f, which is related to the density of free charge n_f by the general equation:

$$Q_f = -q \int_{\text{surface}}^{\text{bulk}} n_f \mathrm{d}x \tag{A.12}$$

As previously, equation (A.12) can be integrated by changing the spatial variable x to the potential V

$$Q_f = -q \int_0^{V_s} \frac{n_f}{F} \mathrm{d}V \tag{A.13}$$

which may also write

$$Q_f = \frac{\varepsilon_s kT n_b}{Q_{tot}} \int_0^{u_s} \frac{\mathrm{e}^u}{f} \mathrm{d}u \tag{A.14}$$

where $n_b = N_c \exp[-(E_c - E_{f0})/kT]$ has already been defined in the text. Here, $f = F/F_s$, and u_s is the value of u at the semiconductor surface. Use has been made of Gauss's law (A.9). Making use of the electric field given by (A.6) we get

$$Q_f = \frac{kT\varepsilon_s n_b}{Q_{tot}} \frac{2l}{2l-1} \left(\mathrm{e}^{u_s} - \mathrm{e}^{u_s/2l}\right) \tag{A.15}$$

In the multiple trapping approximation, the free surface charge is also given by

$$Q_f = -\frac{\mu_{FET}}{\mu_0} C_i(V_g - V_{fb}) \tag{A.16}$$

(A.16) is equivalent to equation (6) of the text. From (A.15) and (A.16), and restricting ourselves to the case where $l \gg 1$, we finally get

$$qV_s = E_c - E_{f0} - kT \ln\left[\frac{2l-1}{2l} \frac{\mu_0 N_c kT\varepsilon_s}{\mu_{FET} C_i^2 (V_g - V_{fb})^2}\right] \tag{A.17}$$

which is indeed very similar to equation (12).

References

[1] Nevin W.A. and Chamberlain G.A., Dark and Photovoltaic Properties of Doped Tetraphenylporphyrin Sandwich Cells 1. Doping Effects and Dark Electrical Properties, *J. Chem. Soc. Faraday Trans. 2* **85** (1989) 1729, and references therein.

[2] Kanicki J., Handbook of Conducting Polymers, T.A. Skotheim Ed. (Marcel Dekker, New York, 1985) Vol. 1.

[3] Burroughes J.H., Bradley D.C.C., Brown A.R., Marks R.N., McKay K., Friend R.H., Burns P.N. and Holmes R.B., Light-Emitting Diodes Based on Conjugated Polymers, *Nature* **341** (1990) 539.

[4] Braun D. and Heeger A.J., Visible Light Emission from Semiconducting Polymer Diodes, *Appl. Phys. Lett.* **58** (1991) 1982.

[5] Ebisawa F., Kurokawa T. and Nara S., Electrical Properties of Polyacetylene-Polysiloxane Interface, *J. Appl. Phys.* **54** (1983) 3255.

[6] Burroughes J.H., Jones C.A. and Friend R.H., Polymer Diodes and Transistors: New Semiconductor Device Physics, *Nature* **335** (1988) 137.

[7] Koezuka H., Tsumura A. and Ando T., Field-effect Transistor with Polythiophene Thin-Film, *Synth. Met.* **18** (1987) 699.

[8] Paloheimo J., Kuivalainen P., Stubb H., Vuorimaa E. and Yli-Lahti P., Molecular Field-Effect Transistors Using Conducting Polymer Langmuir-Blodgett Films, *Appl. Phys. Lett.* **56** (1990) 1157;
Paloheimo J., Punkka E., Stubb H. and Kuivalainen P., Polymer Field-Effect Transistors for Transport Property Studies, Lower Dimensional Systems and Molecular Electronics, R.M. Metzger Ed. (Plenum Press, New York, 1991) p. 635.

[9] Fuchigami H., Tsumura A. and Koezuka H., Poly(thienylene vinylene) Thin-Film Transistor with High Carrier Mobility, *Appl. Phys. Lett.* **63** (1993) 1372.

[10] Guillaud G., Madru R., Al Sadoun M. and Maitrot M., Thin-Film Transistors Based on Nickel Phthalocyanine, *J. Appl. Phys.* **66** (1989) 4554.

[11] Horowitz G., Fichou D., Peng X.Z., Xu Z.G. and Garnier F., A Field-Effect Transistor Based on Conjugated Alpha-Sexithienyl, *Solid State Commun.* **72** (1989) 381;
Horowitz G., Peng X.Z., Fichou D. and Garnier F., The Oligothiophene-Based Field-Effect Transistor: How it Works and How to Improve it, *J. Appl. Phys.* **67** (1990) 528.

[12] Ostoja P., Guerri S., Impronta M., Zabberoni P., Danieli R., Rossini S., Taliani C. and Zamboni R., Instability in Electrical Performance of Organic Semiconductor Devices, *Adv. Mater. Optics Electron.* **1** (1992) 127;
Ostoja P., Guerri S., Rossini S., Servidori M., Taliani C. and Zamboni R., Electrical Characteristics of Field-Effect Transistors Formed with Ordered Alpha-Sexithienyl, *Synth. Met.* **54** (1993) 447.

[13] Waragai K., Akimichi H., Hotta S., Kano H. and Sakaki H., FET Characteristics of Substituted Oligothiophenes with a Series of Polymerization Degrees, *Synth. Met.* **57** (1993) 4053.

[14] Garnier F., Horowitz G., Peng X.Z. and Fichou D., An All-Organic 'Soft' Thin-Film Transistor with Very High Carrier Mobility, *Adv. Mater.* **2** (1990) 592.

[15] Fichou D., Horowitz G., Xu B. and Garnier F., Generation of Stabilized Polarons and Bipolarons on Extended Model Thiophene Oligomers, *Synth. Met.* **41** (1991) 463.

[16] Hotta S. and Waragai K., Solid-State Absorption Spectroscopy of Alkyl-Substituted Oligothiophenes, *J. Phys. Chem.* **97** (1993) 7427.

[17] Kaneto K., Ura S., Yoshino K. and Inuishi Y., Optical and Electrical Properties of Electrochemically Doped n- and p-Type Polythiophenes, *Jap. J. Appl. Phys.* **23** (1984) L189.

[18] Nowak M.J., Rughooputh S.D.D.V., Hotta S. and Heeger A.J., Polarons and Bipolarons on a Conducting Polymer in Solution, *Macromolecules* **20** (1987) 965.

[19] Sze S.M., Physics of Semiconductor Devices, 2nd Edition (John Wiley, New York, 1981).

[20] Horowitz G. and Delannoy P., An Analytical Model for Organic-Based Thin-Film Transistors, *J. Appl. Phys.* **70** (1991) 469.

[21] Le Comber P.G. and Spear W.E., Electronic Transport in Amorphous Silicon Films., *Phys. Rev. Lett.* **25** (1970) 509.

[22] Lampert M.A., Simplified Theory of Space-Charge-Limited Currents in an Insulator with Traps, *Phys. Rev.* **103** (1956) 1648.

[23] Paloheimo J., Isotalo H., Kastner J. and Kuzmany H., Conduction Mechanisms in Undoped Thin Films of C60 and C60/70, *Synth. Met.* **56** (1993) 3185.

[24] Garnier F., Yassar A., Hajlaoui R., Horowitz G., Deloffre F., Servet B., Ries S. and Alnot P., Molecular Engineering of Organic Semiconductors - Design of Self-Assembly Properties in Conjugated Thiophene Oligomers, *J. Am. Chem. Soc.* **115** (1993) 8716.

[25] Spear W.E. and Le Comber P.G., Investigation of the Localised State Distribution in Amorphous Si Films, *J. Non-Cryst. Solids* **8-10** (1972) 727;
Madan A., Le Comber P.G. and Spear W.E., Investigation of the Density of Localized States in a-Si Using the Field-Effect Technique, *J. Non-Cryst. Solids* **20** (1976) 239.

[26] Powell M.J., Analysis of Field-Effect-Conductance Measurements on Amorphous Semiconductors, *Phil. Mag. B* **43** (1981) 93.

[27] Roth S., Hopping Transport in Solids, M. Pollack and B. Shklovkii Eds. (Elsevier Science Publishers, Lausanne, 1991) p. 377.

[28] Servet B., Ries S., Trotel M., Alnot P., Horowitz G. and Garnier F., X-Ray Determination of the Crystal Structure and Orientation of Vacuum Evaporated Sexithiophene Films, *Adv. Mater.* **5** (1993) 461.

[29] Fichou D., Horowitz G., Nishikitani Y. and Garnier F., Conjugated Oligomers for Molecular Electronics: Schottky Diodes on Vacuum Evaporated Films of Alpha-Sexithienyl, *Chemtronics* **3** (1988) 176.

[30] Shur M. and Hack M., Physics of Amorphous Silicon Based Alloy Field-Effect Transistor, *J. Appl. Phys.* **55** (1984) 3831;
Shaw J.G. and Hack M., An Analytical Model for Calculating Trapped Charge in Amorphous Silicon, *J. Appl. Phys.* **64** (1988) 4562;
Shur M., Hack M. and Shaw J.G., A New Analytic Model for Amorphous Thin-Film Transistors, *J. Appl. Phys.* **66** (1989) 3371.

[31] Servet B., Horowitz G., Ries S., Lagorsse O., Alnot P., Yassar A., Deloffre F., Srivastava P., Hajlaoui R., Lang P. and Garnier F., Polymorphism and Charge Transport in Vacuum-Evaporated Sexithiophene Films, *Chem. Mater.* **6** (1994) 1809.

[32] von Bardeleben H.J. and Horowitz G., unpublished.

[33] Karl N., Marktanner J., Stehle R. and Warta W., High-Field Saturation of Charge Carrier Drift Velocities in Ultrapurified Organic Photoconductors, *Synth. Met.* **42** (1991) 2473.

[34] Silinsh E.A., Shlihta G.A. and Jurgis A.J., A Model Description of Charge Carrier Transport Phenomena in Organic Molecular Crystals. I. Polyacene Crystals, *Chem. Phys.* **138** (1989) 347;
Silinsh E.A., Shlihta G.A. and Jurgis A.J., A Model Description of Charge Carrier Transport Phenomena in Organic Molecular Crystals. II. Perylene, *Chem. Phys.* **155** (1991) 389.

[35] Rose A., Concepts in Photoconductivity and Allied Problems (John Wiley & Sons, New York, 1960).